Multi-hazard loss analysis of tall buildings under wind and seismic loads

Ilaria Venanzi [a] and Oren Lavan[b] and Laura Ierimonti [a] and Stefano Fabrizi [a]

[a]Department of Civil and Environmental Engineering, University of Perugia. Via G. Duranti, 93 - 06125 Perugia, Italy. [b]Faculty of Civil and Environmental Engineering, Technion - Israel Institute of Technology, 32000, Haifa, Israel.

ARTICLE HISTORY
Compiled February 6, 2018

ABSTRACT
This paper presents a framework for life-cycle loss estimation for non-structural damage in tall buildings under wind and seismic loads. Life-cycle cost analysis is a useful design tool for decision makers, aimed at predicting monetary losses over the lifetime of a structure, accounting for uncertainties involved in the problem definition. For tall buildings, sensitive to dynamic excitations like earthquake and wind, it can be particularly suitable to base design decisions not only on initial cost and performance but also on future repair expenses. The proposed approach harmonizes the procedures for intervention costs evaluation of structures subjected to multiple-hazards, taking into account the peculiar differences of wind and earthquake, in terms of load characterization, type and evolution of damage. Relative effect of the two hazards on damage to drift- and acceleration-sensitive non-structural elements are examined. The influence of uncertainty in structural damping is also taken into account. It is shown that, although it is commonly believed that the design of a given structure is usually dominated by either winds or earthquakes, when LCC-based design is performed, both winds and earthquakes may be important.

KEYWORDS
Life-cycle cost analysis; Tall buildings; Non-structural damage; Multi-hazard analysis; Hazard curves; Fragility analysis.

1. Introduction

The approach to structural design suggested by Codes' provisions is based on the definition of a deterministic model of the structure and is aimed at verifying that the building is capable of withstanding specific levels of excitations, considered as acceptable worst-cases scenarios. Nowadays, the deterministic design approach has started to be replaced by the fully-probabilistic assessment of the structural performance (Lavan & Avishur, 2013; Spence & Kareem, 2014; Venanzi, 2015). In this context, life-cycle cost analysis (LCCA) is becoming a valid tool as it allows accounting for the effects of uncertainties involved in the design, materials' deterioration, damage of structural and non-structural elements, maintenance and repair interventions during the entire lifetime of the building (Lagaros, 2007; C. Mitropoulou, Lagaros, & Papadrakakis,

CONTACT Ilaria Venanzi. Email: ilaria.venanzi@unipg.it Oren Lavan. Email: lavan@technion.ac.il Laura Ierimonti Email: ierimonti@strutture.unipg.it Email: stefano85net@gmail.com

2015; C. C. Mitropoulou, Lagaros, & Papadrakakis, 2011; Okasha & Frangopol, 2011).

LCCA is well established in earthquake engineering and many contributions have been given in the last decade for developing different loss estimation models (Aslani & Miranda, 2005). The loss assessment method is always based on the PEER equation solution which allows the computation of the probability of exceeding a threshold cost (Ramirez et al., 2012; Ramirez & Miranda, 2012). Many applications of LCCA are devoted to comparing different retrofitting solutions and planning maintenance schemes in existing bridges (Padgett, Dennemann, & Ghosh, 2010; Wang, Zhai, Li, Ni, & Guo, 2015). LCCA is often used in conjunction with optimization methods, with the aim of minimizing the expected life-cycle cost (Barone & Frangopol, 2014; Frangopol & Maute, 2003; Kaveh, Kalateh-Ahani, & Fahimi-Farzam, 2014; Liu, Wen, & Burns, 2004; Puthanpurayil, Lavan, & Dhakal, 2015, 2017).

In wind engineering further efforts still must be made to improve methods and models, although some recent works presented relevant contributions drawing from seismic engineering field (Ierimonti, Caracoglia, Venanzi, & Materazzi, 2017). In Cui and Caracoglia (2015); Seo and Caracoglia (2013), a numerical framework is developed for estimating the life-cycle monetary losses due to wind-induced damage on long-span bridges and tall buildings, respectively. Damage loss estimation for buildings subjected to hurricanes and strong winds were treated by some authors (Bjarnadottir, Li, & Stewart, 2014; Chung, Lin, & Vanmarcke, 2011). The software Hazus-MH, implemented by the Federal Emergency Management Agency (FEMA), estimates potential losses due to hurricanes in the U.S. territory (Vickery et al., 2006). A risk design optimization method for optimizing life-cycle costs and functionality of tall buildings is proposed in G. Li and Hu (2014).

Life-cycle cost analysis proved to be a valid tool also for the performance assessment of structural control systems for vibration mitigation. In Matta (2015) a method for evaluating, in a life-cycle cost perspective, the seismic effectiveness of tuned mass dampers on inelastic building structures is presented. In Taflanidis and Beck (2009), a systematic probabilistic framework is presented for optimization of the life-cycle cost of engineering systems equipped with passive dissipative devices.

In recent years, life-cycle loss estimation methodologies have also been proposed for structures subjected to multiple-hazards. In Asprone, Jalayer, Prota, and Manfredi (2010), a probabilistic model for multi-hazard risk estimation for a reinforced concrete structure subjected to blast threats in the presence of seismic risk is developed. In Jalayer, Asprone, Prota, and Manfredi (2011) a methodology is presented for LCCA of critical infrastructures accounting for uncertainty in the occurrence of future events due to different types of hazard and for deterioration of the structure after a series of events. Y. Li and Van de Lindt (2012) propose a loss-based approach for design of light-frame wood buildings in areas prone to more than one natural hazard. Multi-hazard risk due to earthquakes and hurricanes is considered in Kameshwar and Padgett (2014) for the LCCA of a portfolio of highway bridges. In Mahmoud and Cheng (2017), the life-cycle cost of two different steel buildings under wind and earthquake is examined.

Although some papers have been published on LCCA of structures subjected to multiple hazards, to the Authors' knowledge a gap can be found in literature on LCCA of tall buildings subjected to wind and earthquake. This is probably due to the commonly accepted idea that tall buildings are mainly prone to wind induced damage and do not experience significant losses due to seismic load.

Conversely, the idea at the base of the paper is that also earthquake can contribute to damage to non structural components and therefore, when estimating non structural life cycle losses, it is advantageous to use a LCCA procedure that can account for both

wind and seismic load in a unified manner. Moreover, damage to non-structural components is one of the most important sources of expenses for tall buildings and therefore its estimation deserves particular attention (Miranda, Mosqueda, Retamales, & Pekcan, 2012). Especially high-rise buildings, due to their high slenderness and related high natural period, are mainly prone to serviceability problems and non-structural damage (Priestley, Calvi, & Kowalsky, 2007; Pu, Kasai, & Kashima, 2012).

For these reasons, the main goal of this paper is to present a framework for LCCA of non structural damage in tall buildings subjected to wind and seismic loads. The proposed multi-hazard life-cycle cost assessment methodology accounts for repair costs due to damage of acceleration-sensitive and drift-sensitive non structural components and provides the expected life-cycle cost for multiple-hazards. Also uncertainty in the definition of structural parameters and parameters characterizing the aerodynamic loads can be taken into account.

Numerical analyses, carried out on a benchmark 76-story building subjected to an ensemble of seismic accelerograms and to wind forces measured in the wind tunnel, allow the estimation of the relative influence of the two hazards on the expected lifetime costs. Several parametric analyses showed the effect of structural damping randomness on loss estimation. In addition, the effect of the height of the building on LCC, and in particular on the relative contribution of winds and earthquake to the LCC is examined.

The outline of the paper is as follows. Section 2 presents the proposed framework for multi-hazard life-cycle cost analysis of tall buildings under wind and earthquake. Sections 3 and 4 describe the damage analysis and the hazard analyses for wind and earthquake. Section 5 presents the particular case study examined, while the results of the numerical simulations are presented in Section 6. Parametric analysis to evaluate the influence of uncertainty in structural damping definition are presented in Section 7. Another parametric analysis to show how the building's height influences the relative importance of wind- and earthquake-induced losses is carried out in Section 8. Finally, some concluding remarks are given in Section 9.

2. Multi-Hazard Life-Cycle cost analysis

The framework for multi-hazard LCCA of tall buildings proposed in this study, is based on the following assumptions: 1) the structure is restored to its original condition after each occurrence of damage; 2) multiple hazards, like wind and seismic loads, never occur simultaneously and never act on the damaged structure; 3) maintenance costs are neglected as they do not vary significantly between different structural configurations. Therefore, as they do not give an important contribution to the choice of the best design solution, they are so far neglected in the analyses.

Under these hypotheses, the expected life-cycle cost of a non-structural element over a time period t, which is the design life or the remaining life of a retrofitted structure, can be expressed as follows (Wen, 2001; Wen & Kang, 2001b):

$$E(C) = C_0 + E[\sum_{l=1}^{N} \sum_{j=1}^{k} C_j e^{-\lambda t_l} P_j^l] \tag{1}$$

where $E[.]$ denotes expected value; C_0 is the initial cost; C_j is the cost of jth damage state being reached; l is the loading occurrence number; t_l is the loading occurrence

time; N is the total number of loading occurrences in t; λ is the constant discount rate per year; P_j^l is the probability of exceeding jth damage state given the l-th occurrence of hazard; k is the total number of damage states under consideration.

It is worth noticing that with respect to the original formulation by Wen that considers the probability of limit state crossing, in Equation (1) the probability of exceeding a certain damage state is considered. The use of probability of exceeding a damage state (a level of damage) instead of a limit state (a response threshold) allows accounting for the randomness of damage occurrence given a specific value of structural response.

If the probability of exceeding damage states is time-independent, the expected total cost can be evaluated in closed form as (Wen & Kang, 2001b):

$$E(C) = C_0 + \frac{1 - e^{-\lambda t}}{\lambda} \sum_{j=1}^{k} (C_j \upsilon P_j) \tag{2}$$

where υ is the mean rate of occurrence of the hazard, modeled by a Poisson process, P_j is the probability of exceeding the jth damage state given the occurrence of hazard.

If n hazards types are considered (e.g. wind and earthquake), Equation (2) becomes:

$$E(C) = C_0 + \frac{1 - e^{-\lambda t}}{\lambda} \sum_{j=1}^{k} \sum_{i=1}^{n} (C_j^i \upsilon_i P_j^i) \tag{3}$$

where υ_i is the mean rate of occurrence of the hazard i, P_j^i is the probability of exceeding the jth damage state given the occurrence of hazard i. The total expected cost of the structure in its lifetime is the summation of the expected costs of all the non-structural elements in the structure.

By normalizing the restoration expenses with respect to the initial cost of the structure and limiting the analysis to the occurrence of wind (w) and earthquake (e) hazards, Equation (3) becomes:

$$E(\frac{C - C_0}{C_0}) = \frac{1 - e^{-\lambda t}}{\lambda} [\sum_{j=1}^{k_w} (c_j^w \upsilon_w P_j^w) + \sum_{j=1}^{k_e} (c_j^e \upsilon_e P_j^e)] \tag{4}$$

where $c_j^w = C_j^w / C_0$ and $c_j^e = C_j^e / C_0$ are the ratio of the intervention costs for the jth damage state relative to the initial construction cost for wind and earthquake, k_w and k_e are the number of damage states to be considered for the analysis under wind and seismic load, respectively.

The *cost analysis*, consisting in the solution of Equation (4), requires the computation of the probabilities of exceeding damage thresholds. With this aim, after a preliminary modeling of wind and earthquake hazards, structural analysis and damage analysis have to be performed. A schematic outline of the multi-hazard life-cycle cost analysis procedure is shown in Figure 1. Structural analysis and damage analysis are discussed in Section 3 while hazard analysis for earthquake and wind is discussed in Section 4.

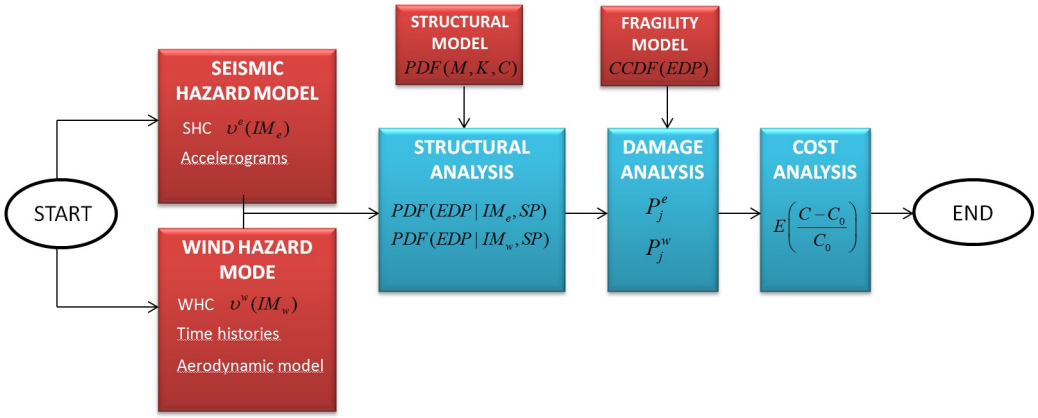

Figure 1. Overview of the proposed multi-hazard life-cycle cost analysis procedure.

3. Structural and damage analysis

For each hazard, *damage analysis* consists in the computation of the probabilities of exceeding damage thresholds by solving the well known PEER equation (Ciampoli, Petrini, & Augusti, 2011; PEER, 2010):

$$P_j^i = \int\int\int\int P(DS_j|EDP)f(EDP|IM_i,SP,IP_i) \\ f(IP_i|IM_i,SP)f(IM_i)f(SP)d(EDP)d(IP_i)d(IM_i)d(SP) \quad (5)$$

where DS_j is the jth damage state; EDP is the vector collecting the engineering demand parameters (i.e. structural response components) provoking the damage; IM_i is the intensity measure of the ith hazard; SP is the vector of the parameters characterizing the structural system; IP_i is the vector of the interaction parameters (aerodynamic and aeroelastic parameters in wind engineering problems); $P(DS_j|EDP)$ is the fragility curve (i.e. the complementary cumulative distribution function of DS_j conditioned to the occurrence of EDP); $f(EDP|IM_i,SP,IP_i)$ is the PDF of EDP conditional on IM_i, SP and IP_i; $f(IP_i|IM_i,SP)$ is the PDF of IP_i conditional on IM_i and SP, $f(IM_i)$ and $f(SP)$ are the PDFs of IM_i and SP, respectively.

Interaction parameters have been introduced in the formulation of the PEER equation for Performance-Based Wind Engineering (PBWE) (Ciampoli et al., 2011; Spence & Kareem, 2014). In PBWE the load modeling requires the definition of the aerodynamic and aeroelastic coefficients which depend on structural shape, structural dynamic characteristics and load intensity. If the interaction parameters are supposed to be deterministic, Equation (5) can be simplified as follows:

$$P_j^i = \int\int\int P(DS_j|EDP)f(EDP|IM_i,SP) \\ f(IM_i)f(SP)d(EDP)d(IM_i)d(SP) \quad (6)$$

Equation (6) can be adopted both in wind engineering problems, if the interaction parameters can be considered deterministic, and in earthquake engineering problems

in which interaction parameters do not exist.

The *structural analysis* leads to the evaluation of the term $f(EDP|IM_i, SP)$. In general, a nonlinear analysis is required. Nonetheless, in some cases a linear analysis can be justified, depending on the building, the excitation characteristics and its intensity.

4. Hazard modeling

4.1. Seismic load

In order to characterize seismic load, it is necessary to have available Seismic Hazard Curve (SHC) which is computed by Probabilistic Seismic Hazard Analysis (PSHA) (Cornell, 1968; McGuire, 1995) and accounts for uncertainties on type of source, distance and ground motion intensity. SHC represents the annual frequency of exceeding a certain intensity measure $\upsilon^e(IM)$, that is related to the annual probability of exceeding at least one event $H^e(IM)$ by the following relationship, provided that the earthquake occurrences are modeled as a Poisson process with a mean occurrence rate of υ^e per year (Gencturk, Hossain, & Lahourpour, 2016):

$$H^e = 1 - e^{-\upsilon_e} \tag{7}$$

The intensity measure IM can be the peak ground acceleration or the spectral acceleration at a selected period. In order to account for randomness of seismic load, it is also necessary to dispose of a set of base accelerograms which are then scaled to match the relevant IM according to the SHC in order to compute probability distributions of response components. Accelerograms can be records of natural earthquakes or can be spectrum-compatible numerically generated. Exploiting Equation (6), the annual probability of exceeding damage state j due to earthquake is:

$$P^e_{aj} = \int\int\int P(DS_j|EDP)\frac{dP(EDP|IM,SP)}{dEDP} \frac{dH^e(IM)}{dIM} f(SP)d(EDP)d(IM)d(SP) \tag{8}$$

and the t-year probability of exceeding damage state j is:

$$P^e_{tj} = 1 - (1 - P^e_{aj})^t \tag{9}$$

Since the earthquake occurrences are modeled as a Poisson process with a mean occurrence rate of ν_e per year, the exceedance probability over a period t is given by Wen and Kang (2001a):

$$P^e_{tj} = 1 - e^{-\upsilon_e P_j t} \tag{10}$$

where P_j is the probability of exceeding a damage state j given the occurrence of a seismic event and t is the service life of the structure. Based on Equations (8) to (10)

and considering the sole seismic hazard, Equation (3) becomes:

$$E(\frac{C-C_0}{C_0}) = \frac{1-e^{-\lambda t}}{\lambda t}\sum_{j=1}^{k}[-c_j^e ln(1-P_{tj}^e)] \tag{11}$$

When the same non-structural element can experience different levels of damage (e.g. slight, moderate or severe), to make sure that the cost associated to the smaller damage is not considered more than once, the actual probability of being at a single level of damage should be computed as follows (Padgett et al., 2010):

$$E(\frac{C-C_0}{C_0}) = \frac{1-e^{-\lambda t}}{\lambda t}\sum_{j=1}^{k} -c_j^e[ln(1-P_{tj}^e) - ln(1-P_{tj+1}^e)] \tag{12}$$

4.2. Wind load

In order to characterize wind load, it is necessary to have available a wind hazard curve for the site and a set of wind load time histories. Wind action on buildings is affected by uncertainties in parameters characterizing the wind field (mean wind velocity, turbulence intensity, dominant wind direction), and parameters characterizing the aerodynamic and aeroelastic properties of the structure (aerodynamic and aeroelastic coefficients). The former are referred to as intensity measure parameters (IM) and the latter as interaction parameters (IP). Therefore, the computation of the probability of exceeding a damage state should account for both the parameters groups as specified in Ciampoli et al. (2011).

In this paper, for the sake of simplicity, the wind mean reference velocity V_{ref} is considered as the only random parameter characterizing the loading intensity and the interaction parameters are considered as deterministic.

The reference wind velocity is the largest annual mean wind speed at 10 meters high in open terrain and in non-hurricane-prone regions it can be well modeled by a Type I extreme value distribution (Gumbel distribution) (Gomes & Vickery, 1977).

In order to have an unique framework for the multi-hazard LCCA, a Wind Hazard Curve (WHC) conceptually similar to the one computed by PSHA is evaluated. WHC for a specific site is obtained by estimation of extreme wind speeds based on in-site recorded wind speed data or can be taken from literature.

Assuming that in the case of wind load characterization, IM is the extreme annual value of the reference mean wind speed, and adopting for V_{ref} the Gumbel probability distribution, WHC is computed as follows:

$$H^w(V_{ref}) = 1 - exp[-exp(\frac{V_{ref}-\mu}{\beta})] \tag{13}$$

where μ and β are related to the mean value and the standard deviation of the distribution.

Following the approach reported in Section 4.2 and using Equations (8) to (10), the expected normalized life-cycle cost is computed by:

$$E(\frac{C-C_0}{C_0}) = \frac{1-e^{-\lambda t}}{\lambda t}\sum_{j=1}^{k} -c_j^w[ln(1-P_{tj}^w) - ln(1-P_{tj+1}^w)] \tag{14}$$

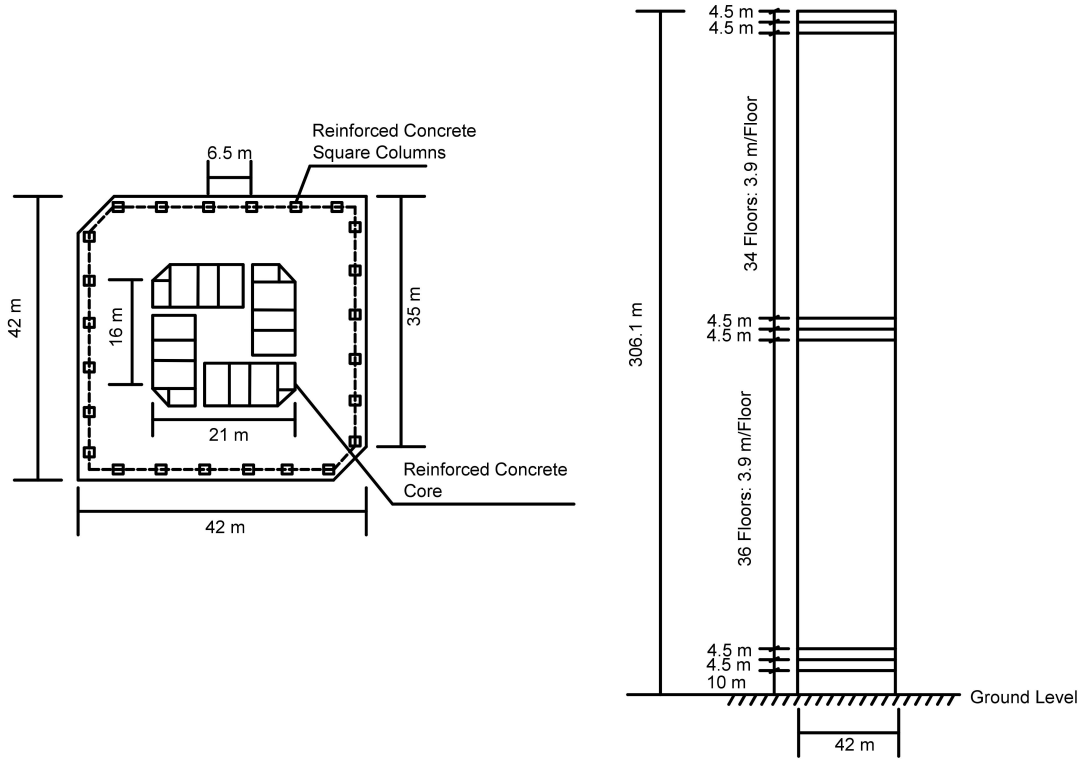

Figure 2. Plan and elevation views of the 76-story building (after Yang et al. (2004)).

5. The case study

5.1. Description of the structure

The structure chosen as case study is the 76-story building, 306 meters high, proposed as benchmark problem for response control under wind load by Yang, Agrawal, Samali, and Wu (2004). Figure 2 shows the plan and elevation views of the structure. The building has a square cross section with chamfer at two corners, constant along the height. It is a reinforced concrete building consisting of a concrete core, designed to resist lateral loads and concrete frames mainly devoted to support gravity loads.

A simplified model of the building is considered, consisting of an Euler-Bernoulli cantilever beam with 76 degrees of freedom, one for each floor. Therefore, only the planar response of the structure is considered. In accordance to the information provided by the benchmark, damping ratio for all modes is 1% and the first two natural periods are 6.25 s and 1.30 s.

5.2. Characterization of seismic load

To characterize seismic load, 20 accelerograms relative to the Los Angeles area, with a 10% probability of exceedance in 50 years, are selected from the PEER NISEE (2017).

Table 1. Parameters of seismic hazard curves

Location	υ^e_{asy}	$S_{a,asy}$	α
Otira	16.54	1.49	29.75
Wellington	321.22	4.04	58.63
Christchurch	37.44	0.33	29.07
Aukland	1368.88	0.68	63.21

These acceleration time histories are then scaled to match the relevant IM according to the hazard curves. Seismic hazard curves are computed according to Bradley, Dhakal, Cubrinovski, Mander, and MacRae (2007) who proposed a hyperbolic model in the double logarithmic plane:

$$ln(\upsilon^e) - ln(\upsilon^e_{asy}) = \frac{\alpha}{ln(S_a) - ln(S_{a,asy})} \tag{15}$$

where υ^e_{asy} and $S_{a,asy}$ are the horizontal and vertical asymptotes, α is a constant and ε is a random variable representing uncertainty.

In the present work a set of hazard curves for the main centers in New Zeeland are adopted (Bradley et al., 2007). Without loss of generality it was chosen to use hazard curves relative to New Zeeland and accelerograms relative to Los Angeles. This was due mainly to the unavailability of information relative to the same area.

Nonetheless, as the selected accelerograms are different in terms of spectral characteristics, they are considered covering a wide range of in site conditions. Curves are expressed in terms of spectral acceleration for a building whose first natural period is $T_1^* = 1.5$ s. As the fundamental period of the tall building is $T_1 = 6.25$ s, the spectral acceleration of the selected hazard curve is then scaled by a factor $\chi = 7.84$. The coefficient χ is defined as:

$$\chi = \frac{E[S_a(T_1^*)]}{E[S_a(T_1)]} \tag{16}$$

where $E[.]$ denotes mean value and is computed considering the set of available accelerograms.

In order to obtain S_a from each accelerogram, the structure has been considered as an equivalent 1 DOF system having $T_1 = 6.25$ s and a mass equal to the first modal mass of the building. The analytical hyperbolic relationships describing the hazard curves are obtained by computing the parameters that appear is Equation (15). The coefficients, computed by non-linear regression in the range $[10^{-5} < \upsilon < 10^{-1}]$, are reported in Table 1. Seismic hazard curves adopted in the simulations are shown in Figure 3.

5.3. Characterization of wind load

Wind loads on the benchmark building were obtained by tests performed in the boundary layer wind tunnel facility at the Department of Civil Engineering at University of Sidney, Australia (Samali, Kwok, Wood, & Yang, 2004). The rigid model of the building had a length scale of 1:400. Wind pressures were recorded for 27 s, corresponding to about 1 h in prototype scale. Pressure coefficients were integrated and

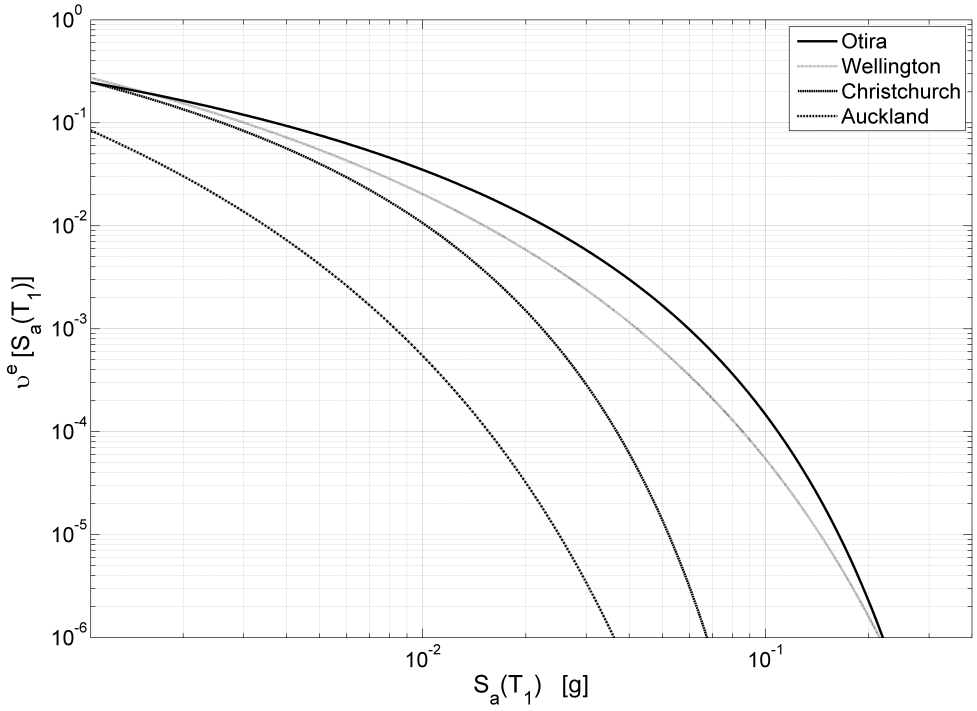

Figure 3. Seismic hazard curves adopted in the simulations.

converted into across-wind forces at each story. The mean wind velocity at the top of the building was 47.25 m/s corresponding to 13.5 m/s reference wind velocity at 10 m above ground, by considering a power law exponent of 0.365. As the benchmark provides only acrosswind forces, a planar analysis in the direction orthogonal to the mean wind speed direction was carried out.

With the aim of having different realizations of the wind load stochastic process, the 76 time histories of the across-wind forces are divided into 20 time histories each one having a duration of 10 minutes, allowing superposition between adjacent time windows. For the purpose of the life-cycle analysis, the wind hazard curve is computed by Equation (13). The mean values of annual maxima of wind velocity are taken by wind load Code of New Zeeland (AZ-NZS, 2011) for the considered locations and for a return period of 1 year. The 3–seconds gust reference wind speeds provided by the Code are transformed into 10–minutes gust values, leading to the mean reference velocities reported in Table 2. In absence of information on standard deviation of the reference wind velocity, a coefficient of variation of 0.2 was assumed for all the sites. Figure 4 shows the wind hazard curve adopted in the simulations.

6. Numerical analyses

6.1. Structural analysis

As stated in Section 3, the structural analysis can be linear or nonlinear, depending on the characteristics of the building and the excitation. The assumption of linear behavior is commonly accepted for wind-excited tall buildings, that usually remain

Table 2. Parameters of wind hazard curves

Location	$V_{ref}^{3s-gust}$ (m/s)	$V_{ref}^{10min-gust}$ (m/s)	CoV
Otira	30	20.1	0.2
Wellington	34	22.8	0.2
Christchurch	30	20.1	0.2
Auckland	30	20.1	0.2

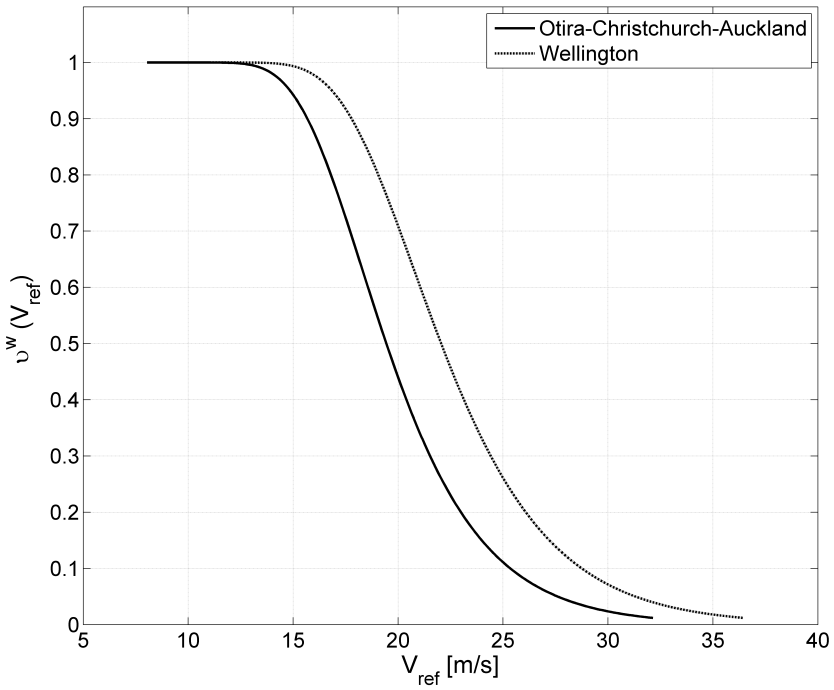

Figure 4. Wind hazard curves adopted in the simulations.

elastic under wind loading.

Experience shows that many tall buildings may remain linear also under seismic excitations (Pu et al., 2012) but there are cases in which nonlinear analysis is advisable (Hart & Jain, 2014; Zhou & Xu, 2007). Therefore, it is not possible to make a general hypothesis and the linearity has to be checked case by case. The main advantage of the adoption of linear analysis is that it is not necessary to compute $f(EDP|IM_i, SP)$ for each IM but it is sufficient to properly scale the $EDPs$, with a consequent benefit in terms of computational effort.

For the selected case study, the linear analysis is adopted. To check the assumption of linear behavior, preliminary structural analyses under the selected seismic accelerograms are carried out. In particular, maximum bending moments at the base of the internal core are used to verify that the related curvatures are smaller than the one corresponding to elastic limit.

Results obtained considering full stiffness and cracked stiffness reduced by 50%, as usually done in order to account for the presence of cracks (Breccolotti, Materazzi, & Venanzi, 2008), show that the central core does not experience yielding. Then, the contribution of the various lateral load resisting systems (central core and frames) to the lateral stiffness of the building is assessed. This is done in two ways. First, the deformed shape of the building under a uniform lateral static load is obtained. This deformed shape is found to be similar to that of a wall structure. Furthermore, based on Yang et al. (2004) reasonable sizes of the elements are assumed and the parameter controlling the behaviour of wall-frame structures, αH, was estimated to be around 0.5 (Stafford Smith & Coull, 1991). This implies that the frame has a very small effect on the behaviour of the structure. Thus, assuming a linear behaviour of this frame is not expected to lead to large errors in the prediction of the behaviour of the structure, even under strong events.

Based on the above analyses, it can be stated that for the specific example structure, the estimation of the response using linear analysis is expected to lead to reasonable predictions, even for strong ground motions. Even if a strong earthquake occurs, leading to damage to outer frames, the probability of occurrence of such a strong earthquake is small. The contribution of such rare events to the life-cycle cost is not expected to be large. Therefore, a small error in the prediction of the behavior of the structure under these rare events, due to the use of linear analysis, is expected to lead to second order inaccuracies that may be negligible. To compute the structural response, the linear dynamic analysis is carried out adopting the Newmark-beta method.

As the proposed procedure is devoted to the evaluation of life-cycle costs of damage to non-structural components, the interstory drift ratio (IDR) and the peak acceleration (a) are chosen as engineering demand parameters (EDPs). In this first phase of the study the structural parameters (SPs) and the interaction parameters (IPs) are considered as deterministic. Analyses are carried out adopting a damping ratio of 1% of the critical for each mode. The subsequent step for the application of the procedure is the computation of the probability density functions of EDPs, according to Equation (8). With this aim, the structural response is calculated by using the 20 accelerograms and the 20 wind load time histories in order to derive the mean values and standard deviations of the peak response under earthquake ($\overline{EDP}^e$) and wind ($\overline{EDP}^w$). In the case of seismic load, the 20 accelerograms are preliminary scaled to have the same reference value of peak spectral acceleration at the first natural period of the building $\overline{S}_a(T_1)$, which is the mean value (among the 20 accelerograms) of $S_a(T_1)$. In the case of wind load, the 20 time histories are preliminary scaled to have

the same reference value of mean wind velocity $\overline{V}_{ref}$, which is different from the one used in the wind tunnel tests.

As the building response is linear, the peak EDP^e and EDP^w are computed in correspondence of each intensity level ($S_a(T_1)$ and V_{ref}) by scaling the mean EDPs as follows:

$$EDP^e|S_a(T_1) = \overline{EDP}^e \frac{S_a(T_1)}{\overline{S}_a(T_1)} \tag{17}$$

$$EDP^w|V = \overline{EDP}^w (\frac{V_{ref}}{\overline{V}_{ref}})^2 \tag{18}$$

Then, the mean values and the standard deviations of EDP^e and EDP^w for each hazard intensity, are used to evaluate the probability density functions, assuming for the EDPs a lognormal distribution.
In principle, the linear scaling of the response cannot be done for wind excited structures, also in case of elastic structural behavior. This is due to the fact that the cross-correlation between the different time histories of the multivariate process representing the wind field depends in a non-linear manner from the mean wind velocity, then as the mean wind intensity increases, the cross-correlation does not remain the same (Di Paola, 1998).

Nevertheless, when wind tunnel records are adopted to characterize the wind load on prismatic tall buildings, it is commonly adopted the hypothesis that the wind field, i. e. the pressure distribution induced by wind on the building's surface does not change with the change of the reference wind velocity.

Equations (18) cannot be used in the case of adoption of nonlinear analysis and the probability distributions of EDP^e and EDP^w must be carried out in correspondence of each value of the intensity measures $S_a(T_1)$ and V_{ref}.

6.2. Damage and cost analyses

A crucial issue for the application of the procedure is the choice of fragility information for wind and earthquake, i.e. the characterization of the probability of exceeding a damage state conditioned to the occurrence of a specific value of an engineering demand parameter, $P(DS_j|EDP)$. As wind and earthquake are different in terms of load duration and power spectral density, it seems reasonable that fragility data for non-structural components do not coincide for the two hazards. Nonetheless, to Authors' knowledge, fragility curves for non-structural components of tall buildings subjected to wind loads are still not available.

To overcome this problem, many authors have avoided damage analysis and have limited the analysis to the computation of the probability of exceeding threshold limit states (Ciampoli et al., 2011; Cui & Caracoglia, 2015; Spence & Kareem, 2014). Some other Authors refer to fragility curves taken by seismic engineering or adopt fragility curves in terms of intensity measures of the two different hazards taken by literature (Kameshwar & Padgett, 2014; Y. Li & Van de Lindt, 2012).

In the present work, the same fragility data in terms of engineering demand parameters are chosen for wind and earthquake. They are taken from the report by Aslani and Miranda (2005), that provides statistical parameters for lognormal fragility functions of generic non-structural drift-sensitive and acceleration-sensitive components.

In particular, the mean values of interstory drift and acceleration (IDR_m and a_m)

Table 3. Statistical parameters for fragility functions of non-structural drift-sensitive components Aslani and Miranda (2005).

Damage level	IDR_m (%)	σ_{IDR}
DS1-IDR: slight	0.4	0.5
DS2-IDR: moderate	0.8	0.5
DS3-IDR: extensive	2.5	0.5
DS4-IDR: complete	5.0	0.5

Table 4. Statistical parameters for fragility functions of non-structural acceleration-sensitive components (Aslani & Miranda, 2005).

Damage level	a_m (g)	σ_a
DS1-a: slight	0.25	0.6
DS2-a: moderate	0.5	0.6
DS3-a: extensive	1.0	0.6
DS4-a: complete	2.0	0.6

and the corresponding standard deviations (σ_{IDR} and σ_a) used to evaluate the fragility curves are reported in Tables 3 and 4. Figure 5 illustrates the fragility functions for drift-sensitive and acceleration-sensitive components and for different levels of damage severity. Cost ratios, that appear in Equations (12) and (14), are the mean values of the distributions reported in Aslani and Miranda (2005) and are shown in Table 5.

6.3. Results

Numerical analyses adopting the proposed multi-hazard life-cycle loss assessment procedure are carried out for the four centers of Otira, Wellington, Christchurch and Auckland, in New Zeeland. Regarding the seismic load, each one of the sites is characterized by a different hazard curve as discussed in Section 5.2.

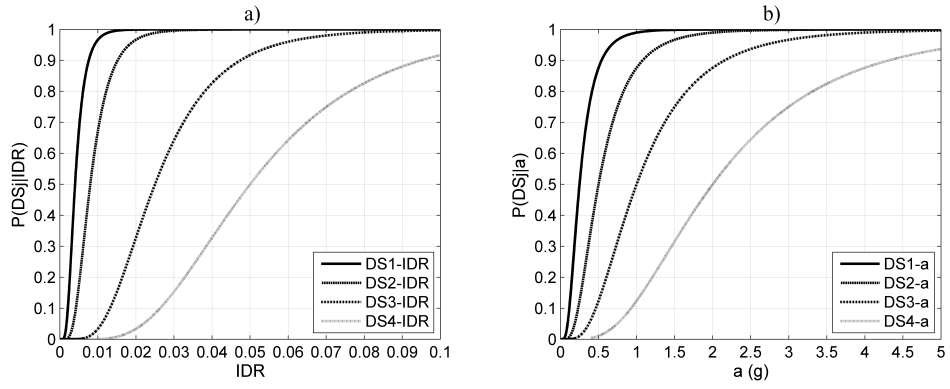

Figure 5. Fragility functions for drift-sensitive components (a) and acceleration-sensitive components (b), for different levels of damage severity.

Table 5. Cost ratios for damage to drift-sensitive and acceleration-sensitive components (Aslani & Miranda, 2005).

Damage level	c_{IDR}	c_a
DS1: slight	0.025	0.02
DS2: moderate	0.1	0.12
DS3: extensive	0.6	0.36
DS4: complete	1.2	1.2

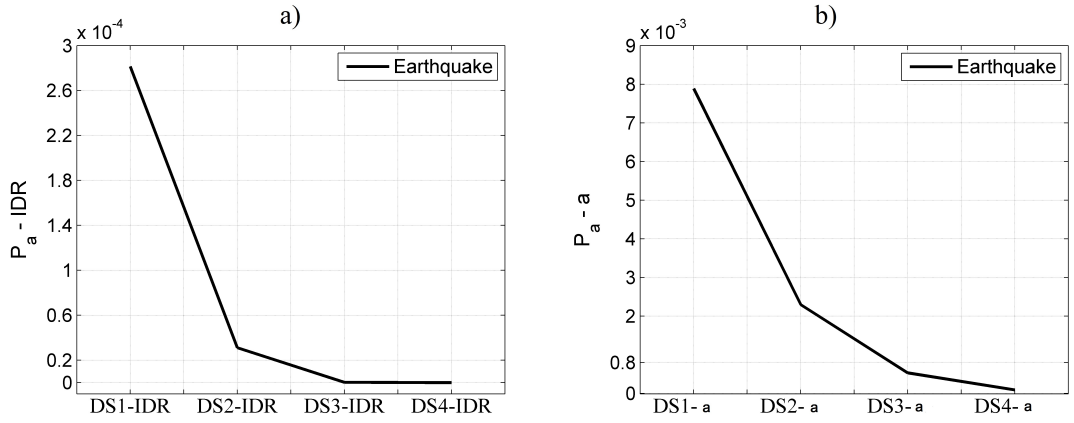

Figure 6. Annual probability of exceeding different levels of drift-dependent damage (a) and acceleration dependent damage (b) at the 76th floor under seismic load for the Auckland site.

Concerning the wind load, three of the sites, Otira, Christchurch and Auckland are characterized by the same wind hazard curve while the city of Wellington is characterized by a higher risk (Section 5.3). For each location, analyses are carried out to evaluate general damages to drift-sensitive components (DS-IDR) and general damages to acceleration sensitive components (DS-a). Moreover, for each damage state, four different damage severities are taken into account.

Results show that as the damage severity increases, the annual probability of exceeding the selected damage state decreases. This trend is shown in Figure 6, reporting the annual probability of exceeding different levels of drift-dependent and acceleration-dependent damage at the 76th floor under seismic load for the Auckland site, which has been computed by exploiting Equation (8).

Figure 7 shows the annual probability of exceeding extensive damage at the 76th floor under wind and earthquake for the four locations. In particular, Figure 7a is referred to drift-sensitive components (DS3-IDR) and Figure 7b to acceleration-sensitive components (DS3-a).

It is possible to observe that wind load leads probability of damage occurrence comparable to earthquake in drift-sensitive components while seismic load leads to higher probability of damage occurrence in acceleration-sensitive components. This can be ascribed to the contribution of higher modes to the seismic response of tall buildings, that is more significant than their contribution to wind response. This result is also confirmed in Aly and Abburu (2015). As further confirmation, high accelerations in real tall buildings were observed in response to the 2011 Tohoku earthquake, and shown to be due to higher mode effects (Pu et al., 2012).

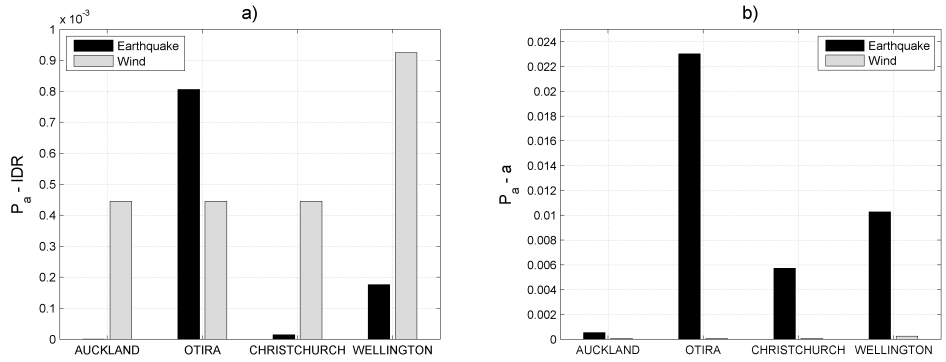

Figure 7. Annual probability of exceeding DS3-IDR (a) and DS3-a (b) at the 76th floor under wind and earthquake for the four locations.

Table 6. Annual probability of exceeding damage states at the 76th floor for Auckland centre.

Damage level	Earthquake		Wind	
	DS-IDR	DS-a	DS-IDR	DS-a
DS1	3.26E-04	1.18E-02	3.65E-01	2.78E-02
DS2	3.73E-05	3.90E-03	7.48E-02	2.20E-03
DS3	2.94E-07	1.00E-03	4.50E-04	6.14E-05
DS4	5.53E-09	2.02E-04	2.87E-06	6.73E-07

Similar results are shown in Table 6 that summarizes the annual probabilities of exceeding each damage state under wind and earthquake at the top floor for Auckland center. Table 6 shows that as the level of damage increases, annual probability of exceeding damage decreases. Moreover, acceleration-dependent damage due to earthquake has higher probability of occurrence than damage due to wind.

Figure 8 shows the distribution over the height of the building of the annual probability of exceeding damage states DS3-IDR and DS3-a for wind and earthquake. Probabilities increase with the height, following the corresponding trend of peak interstory drifts and peak accelerations. It is evident the contribution of higher modes on the distribution of the probability of exceeding acceleration-dependent damage under earthquake.

Expected normalized repair costs are computed for earthquake and wind using Equations (12) and (14), respectively. Figure 9 shows the expected normalized life-cycle costs of drift-dependent (Figure 9a) and acceleration-dependent damages (Figure 9b) for the four sites and for a lifetime of 50 years.

Drift-related costs due to wind are greater that those due to earthquake for all the four considered sites while acceleration-related costs due to earthquake are significantly higher than those due to wind. Therefore, results in terms of costs do not perfectly reflect results in terms of probability of exceedance shown in Figure 8. This is due to the fact that the total expected costs shown in Figure 9 are the sum of costs due to all types of damages (from DS1 to DS4). Results also show that costs related to inter-story drift represent the largest percentage of total repair costs of the building for all the selected locations.

Different expected building's life durations are investigated to assess their influence on life-cycle costs. Figure 10 shows the results in terms of total normalized expected

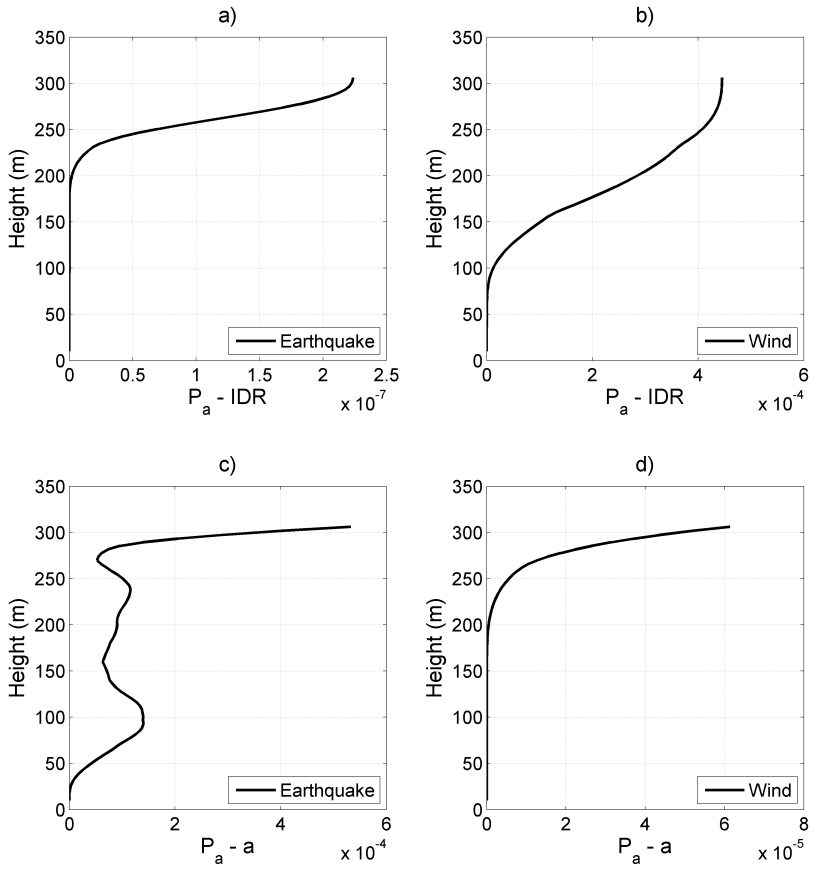

Figure 8. Annual probability of exceeding DS3-IDR and DS3-a for wind and earthquake as a function of the floors' height for Auckland centre.

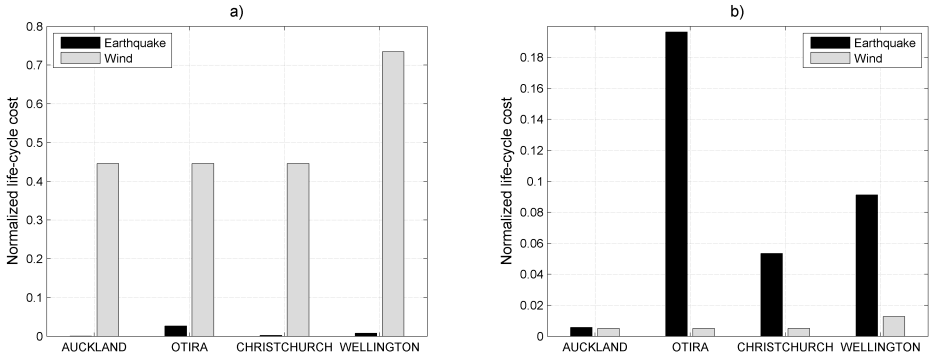

Figure 9. Expected normalized life-cycle costs of drift-dependent (a) and acceleration dependent damages (b).

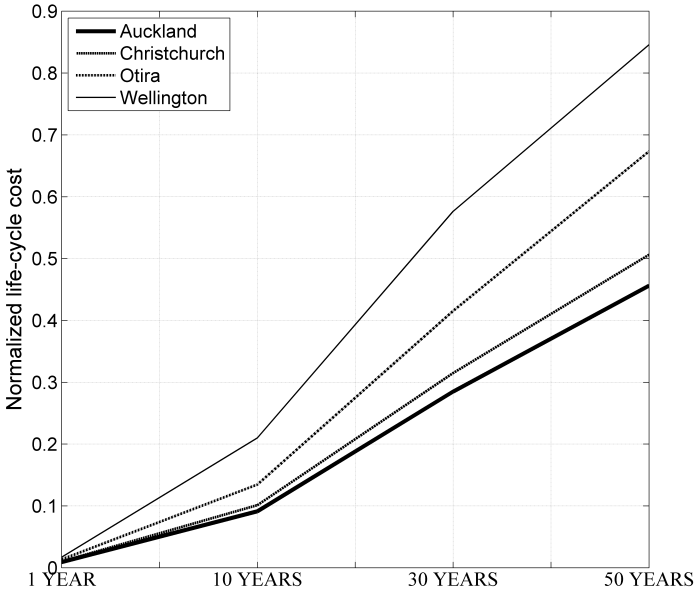

Figure 10. Dependency of expected normalized life-cycle cost on lifetime.

costs for the four locations and for building's life of 1, 10, 30 and 50 years. Costs are obtained by summing up those due to wind and to earthquake and by averaging values over all the floors.

As expected, costs increase significantly with lifetime and the increase depends on the location. The maximum cost is expected for the city of Wellington, where wind-induced drift-dependent damages are highest. Being equal the wind hazard intensity (in the cities of Christchurch, Otira and Auckland), costs increase with seismic hazard.

7. Influence of uncertainty on structural damping

It is well known that damping is the most uncertain parameter among those characterizing the dynamic response. In slender structures, like high-rise buildings, the correct estimate of structural damping is a crucial issue. Major sources of damping in tall buildings, which are expected to remain in linear range, are material damping and friction damping which are related to molecular interaction between the material and to friction between members and connections, respectively (Aquino & Tamura, 2013; Kanduri & Morrow, 1996). Also aerodynamic damping can be experienced by buildings vibrating in air flow. It represents a source of positive damping in low to moderate wind speeds and can play a minor role in vibration reduction (Venanzi & Materazzi, 2012).

Typically, a viscous damping model is used in engineering practice as it leads to a linear equation of motion. In absence of full-scale measurement on the considered building, the modal damping ratios are chosen from Codes on the basis of the material of construction (steel-framed, reinforced concrete, steel-framed reinforced concrete) or

taken from full-scale data available in literature (Fukuwa, Nishizaka, Yagi, Tanaka, & Tamura, 1996; Satake, Suda, Arakawa, Sasaki, & Tamura, 2003). Several authors agree that structural damping is dependent on natural frequency and response amplitude (Çelebi, 1996). Damping predictors based on full-scale data have been proposed, among others, by Jeary (1986); Lagomarsino (1993); Satake et al. (2003). All models include frequency-dependent and amplitude-dependent terms but their application is limited to a specific range of buildings. In this Section, the uncertainty in structural damping is included in life-cycle cost estimation. Damping ratio is considered as the uncertain structural parameter (SP) which appears in Equation (6).

To solve the integral, the probability distribution of the uncertain structural parameter $f(SP)$ must be selected. The lognormal distribution is here considered to characterize randomness of damping ratio. The mean value is $\xi_m = 1\%$ and the coefficient of variation is varied from 0.1 to 0.4 with increments of 0.1 (Kanduri & Morrow, 1996). The Rayleigh model is adopted to compute the viscous damping matrix of the structure. Figure 11 shows the results of numerical analyses with uncertain damping ratio. In particular, it reports the ratios between the annual probabilities of exceeding different levels of damage computed with random ξ and the corresponding probabilities obtained with deterministic damping ratio, relative to the Auckland site. The deterministic damping ratio is the mean value of the probability distributions of ξ and is equal to 1%. It is possible to observe that ratio of probabilities increase with the damage severity, showing that the influence of considering the damping ratio as an uncertain value is greater for high levels of damage. Moreover Figure 11 highlights that the higher is the coefficient of variation that characterizes the probability distribution of ξ, the greater is the influence of variable damping ratio. Probabilities of exceeding acceleration-dependent damages are more strongly dependant of CoV than probabilities of exceeding drift-dependent damages.

Figure 12 shows the expected life-cycle total costs (for both wind and earthquake) as a function of the CoV for wind and earthquake, referred to the Auckland site. Costs are normalized with respect to the costs obtained with the deterministic damping ratio of 1%, corresponding to the mean value of the probability distributions.

Results in terms of costs reflect those in terms of probability: i) costs increase with the coefficient of variation; ii) costs obtained with the constant average damping ratio are intermediate between those obtained with the various CoV, except for the case of drift-dependent damage under wind (where deterministic cost is smaller) and the case of acceleration-dependent damage under earthquake (where the deterministic cost is higher); iii) the choice of the CoV has a greater effect on the cost related to accelerations than on those related to drifts.

8. Influence of building's height on Life-Cycle Cost

The influences on LCC of type of loading, type of damage and building's location have been previously investigated. In this Section, parametric analyses are carried out to assess what is the influence of building's height on the LCC of tall buildings subjected to multiple hazards.

8.1. Buildings' design

Several tall buildings have been considered having height ranging from H=100 m to H=300 m with 10 meters increments. They have square cross section with side length

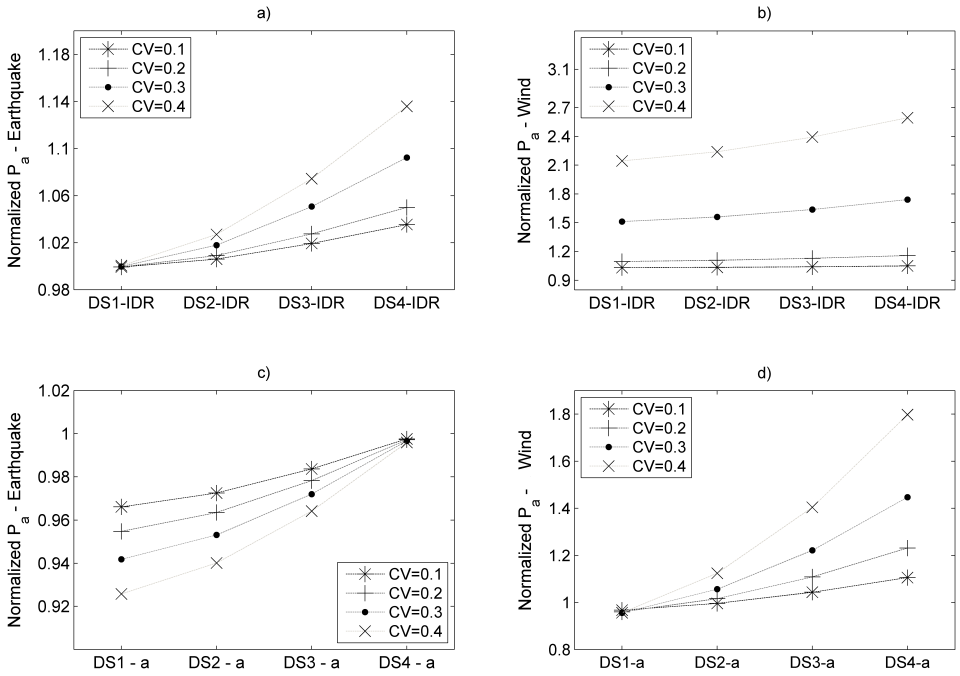

Figure 11. Ratios between annual probability of exceeding damage states computed with uncertain damping ratio and the corresponding probabilities obtained with deterministic damping ratio (Auckland).

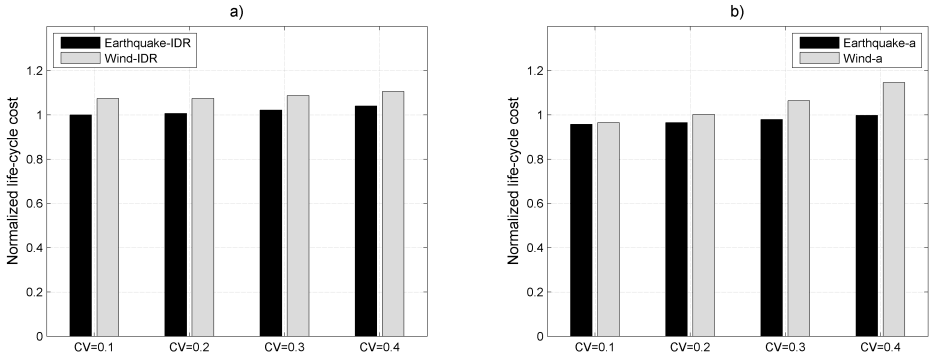

Figure 12. Expected life-cycle costs normalized with respect to the corresponding costs obtained with deterministic damping ratios (Auckland).

30 m. To compute the lumped mass matrix a mass equal to 1 ton/m^2 is considered. To compute the stiffness matrix, each structure is modeled as a cantilever beam with shear walls. The equivalent flexural stiffness is considered constant along the height. To obtain the flexural stiffness EI, the relationship between the flexural stiffness and the natural period of vibration of a Euler-Bernoulli beam T is adopted:

$$EI = (\frac{2\pi}{3.516})^2 m \frac{H^4}{T^2} \tag{19}$$

where m is the building's mass per unit height. Without loss of generality, the natural period is computed according to "Eurocode 8: Design of structures for earthquake resistance Part 1: General rules, seismic actions and rules for buildings" (2004):

$$T = 0.085 H^{0.75} \tag{20}$$

The P-delta effect is taken into account by adding the structural geometric stiffness matrix to the structural stiffness matrix, as in Rutenberg (1981). A damping ratio of 1% for each mode is considered. The damping matrix is computed from mass and stiffness matrix, by adopting the Rayleigh assumption.

8.2. Life-Cycle Cost analysis

The life-cycle cost analysis procedure is applied to investigate the influence of building's height on LCC. To characterize earthquake and wind hazards, the sets of time histories and the hazard curves described in Sections 5.2 and 5.3 are used. Fragility curves for acceleration-induced damage and drift-induced damage adopted in the previous Sections are used.

Figure 13 shows the results obtained under earthquake for the city of Christchurch. In particular, Figures 13a)-b) report the annual probability of exceeding DS3-a and DS3-IDR and Figures 13c)-d) show the corresponding expected normalized Life-Cycle Costs. Figure 14 shows the same results in terms of annual probability and expected LCC, obtained under wind. The three lines in each graph are representative of different stiffnesses of the buildings: the normal stiffness, obtained with Equations (19) and (20), a stiffness increased by 30% and a stiffness decreased by 30%. As the height increases, the annual damage probability decreases under earthquake and increases under wind. The LCC shows a similar trend. The effect of stiffness variation is more pronounced for wind then for earthquake and increases under wind with the height of the building.

The trends shown in Figures 13-14 imply that, for shorter buildings earthquake loss may dominate the design and wind-related loss may be negligible. Similarly, for taller buildings wind may dominate the design and earthquake-related loss may be negligible. There is a relatively large range of structures of intermediate height where both winds and earthquakes contribute considerably to the LCC. In these cases, a design for only one of the hazards may not be adequate from a LCC perspective.

It must be pointed out that in real buildings the initial cost of acceleration-sensitive non-structural components and the initial cost of drift-sensitive non-structural components may be different. In a specific building the cost of acceleration-sensitive components can be a percentage (α) of the cost of drift-sensitive components and this percentage changes from building to building. This will reflect on the relative LCC

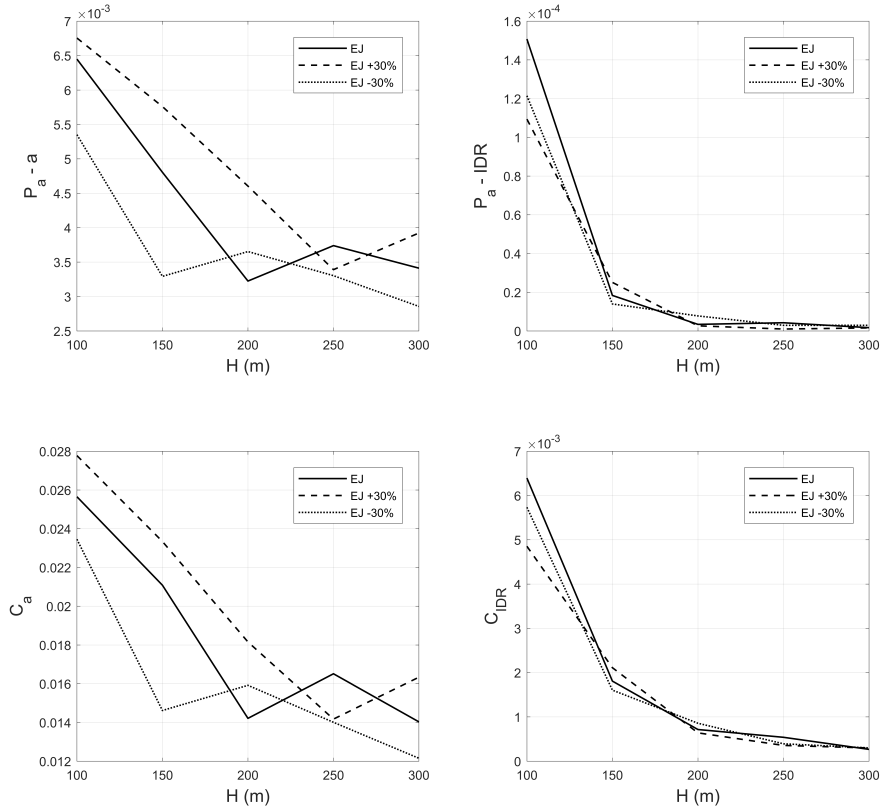

Figure 13. Annual probability of exceeding DS3-a (a), DS3-IDR (b) due to earthquake; earthquake-induced costs related to acceleration (c) and earthquake-induced costs related to drift (d) (Christchurch).

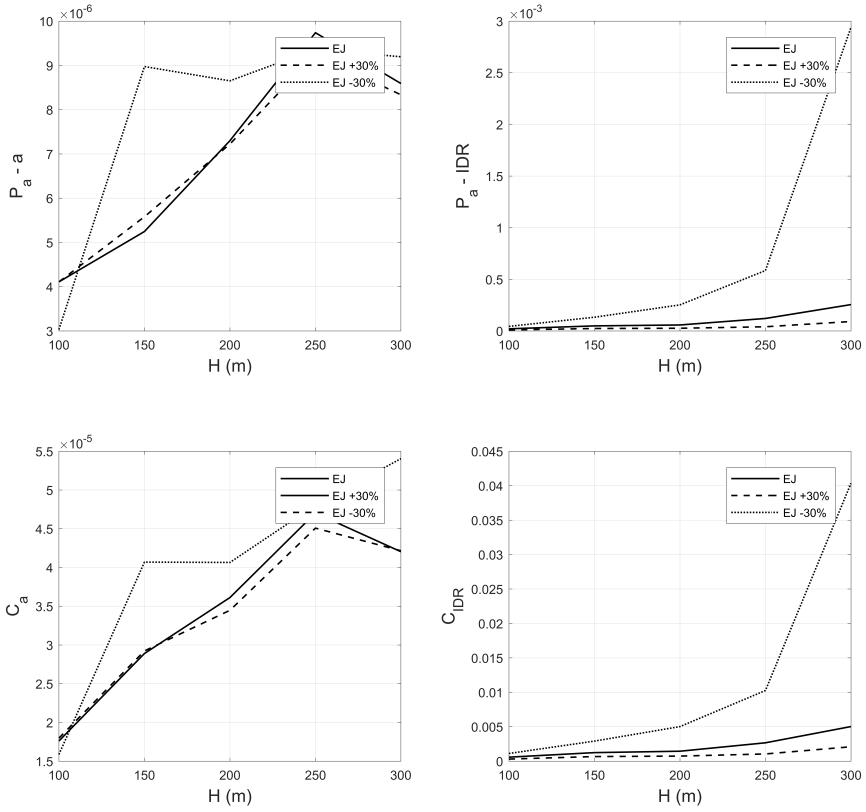

Figure 14. Annual probability of exceeding DS3-a (a), DS3-IDR (b) due to wind; wind-induced costs related to acceleration (c) and wind-induced costs related to drift (d) (Christchurch).

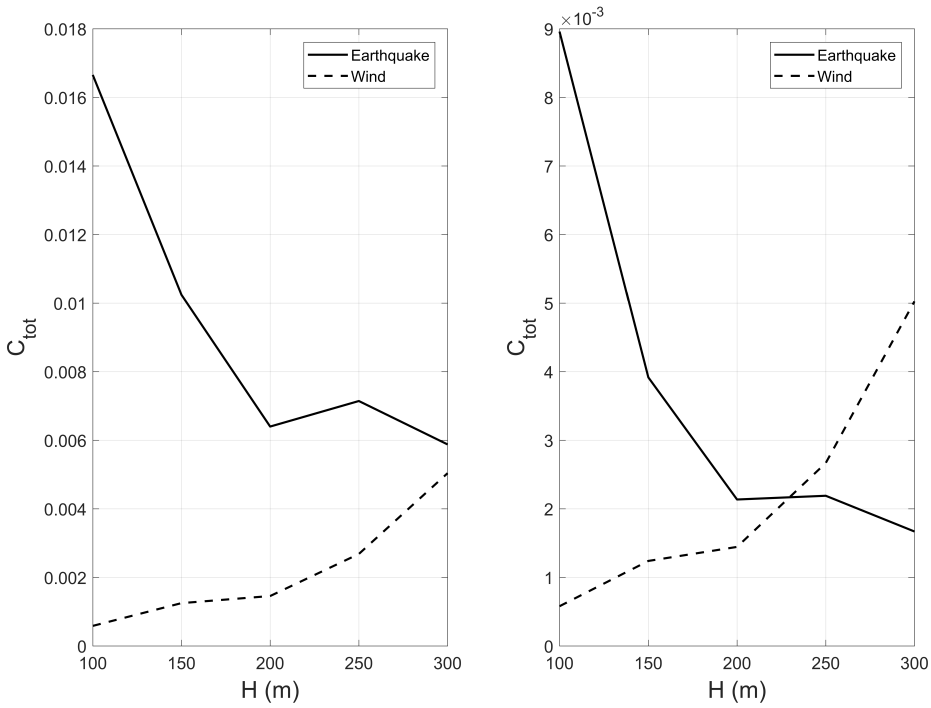

Figure 15. Comparison between total costs for earthquake and wind: $\alpha = 0.4$ (a); $\alpha = 0.1$ (b) (Christchurch).

due to winds and earthquakes.

Figure 15 shows the comparison between the total expected normalized LCC obtained under wind and earthquake. As the height increases, the cost induced by wind increases with height while cost induced by earthquake reduces with height. In particular, results shown in Figure 15(a) are obtained for α=0.4 and those in Figure 15(b) are obtained for α=0.1. It can be observed that the height at which the loss due to wind and the loss due to earthquake intersect depends on the relative total cost of drift-sensitive versus acceleration-sensitive components in the building.

9. Conclusions

In this paper a framework for Life-Cycle Cost Analysis of tall buildings subjected to wind and seismic loads is presented. The procedure uses wind and seismic hazard curves for the specific site of the building and provides the expected normalized value of repair costs of non-structural elements during lifetime.

Several life-cycle cost analyses are carried out on a tall building considered located in four different cities of New Zeeland. Results show that in order to have a correct estimate of the life-cycle cost of a building it is not possible to neglect expenses related to repair of non-structural components which are of the same order of magnitude of initial costs.

Results also show that wind load produces higher costs related to drift-dependent damages then seismic load. Conversely, earthquake produces higher costs related to acceleration-dependent damages then wind load. This is explained by the higher modes contribution, that is more significant in seismic loading, and highly affects the accel-

eration response. The life-cycle cost increases with the duration of life-cycle and is strictly dependent on the hazards' characteristics of the site.

Parametric analyses carried out to assess the influence of uncertainty in structural damping show that the choice of the probability distribution significantly affects life-cycle costs, especially those related to acceleration-dependent damages. Neglecting damping randomness leads to important approximations in life-cycle cost estimation.

Further sensitivity analyses allow to evaluate the effect of building's height on the LCC. The wind-induced non-structural losses increase with height while the earthquake-induced losses show an opposite trend. The height at which the loss due to wind and the loss due to earthquake intersect depends on the relative total cost of drift-sensitive versus acceleration-sensitive components in the building.

References

Aly, A., & Abburu, S. (2015). On the design of high-rise buildings for multihazard: Fundamental differences between wind and earthquake demand. *Shock and Vibration*, *2015*(148681).

Aquino, R., & Tamura, Y. (2013). On stick-slip phenomenon as primary mechanism behind structural damping in wind-resistant design applications. *Journal of Wind Engineering and Industrial Aerodynamics*, *115*, 121–136.

Aslani, H., & Miranda, E. (2005). *Probabilistic earthquake loss estimation and loss disaggregation in buildings* (Tech. Rep. No. 157). The John A. Blume Earthquake Engineering Center.

Asprone, D., Jalayer, F., Prota, A., & Manfredi, G. (2010). Proposal of a probabilistic model for multi-hazard risk assessment of structures in seismic zones subjected to blast for the limit state of collapse. *Structural Safety*, *32*, 25–34.

AZ-NZS. (2011). Australian-New Zeeland Standard (AZ–NZS 1170-2), Structural design actions - part 2: Wind actions.

Barone, G., & Frangopol, D. (2014). Life-cycle maintenance of deteriorating structures by multi-objective optimization involving reliability, risk, availability, hazard and cost. *Structural Safety*, *48*, 40–50.

Bjarnadottir, S., Li, Y., & Stewart, M. (2014). Regional loss estimation due to hurricane wind and hurricane-induced surge considering climate variability. *Structure and Infrastructure Engineering*, *10*(11), 1369–1384.

Bradley, B., Dhakal, R., Cubrinovski, M., Mander, J., & MacRae, G. (2007). Improved seismic hazard model with application to probabilistic seismic demand analysis. *Earthquake Engineering and Structural Dynamics*, *36*, 2211–2225.

Breccolotti, M., Materazzi, A., & Venanzi, I. (2008). Identification of the nonlinear behaviour of a cracked RC beam through the statistical analysis of the dynamic response. *Structural Control and Health Monitoring*, *15*(3), 416–435.

Çelebi, M. (1996). Comparison of damping in buildings under low-amplitude and strong motions. *Journal of Wind Engineering and Industrial Aerodynamics*, *59*, 309–323.

Chung, Y., Lin, N., & Vanmarcke, E. (2011). Hurricane damage and loss estimation using an integrated vulnerability model. *Natural Hazards Review*, *12*(4), 184–189.

Ciampoli, M., Petrini, F., & Augusti, G. (2011). Performance-based wind engineering: towards a general procedure. *Structural Safety*, *32*, 367–378.

Cornell, C. (1968). Engineering seismic risk analysis. *Bulletin of the Seismological Society of America*, *58*(5), 1583–1606.

Cui, W., & Caracoglia, L. (2015). Simulation and analysis of intervention costs due to wind induced damage on tall buildings. *Engineering Structures*, *87*, 183–197.

Di Paola, M. (1998). Digital simulation of wind field velocity. *Journal of Wind Engineering and Industrial Aerodynamics*, *74–76*, 91-109.

Eurocode 8: Design of structures for earthquake resistance part 1: General rules, seismic actions and rules for buildings. (2004).

Frangopol, D., & Maute, K. (2003). Life-cycle reliability-based optimization of civil and aerospace structures. *Computers and Structures*, *81*(7), 397–410.

Fukuwa, N., Nishizaka, R., Yagi, S., Tanaka, K., & Tamura, Y. (1996). Field measurement of damping and natural frequency of an actual steel-framed building over a wide range of amplitudes. *Journal of Wind Engineering and Industrial Aerodynamics*, *59*, 325–347.

Gencturk, B., Hossain, K., & Lahourpour, S. (2016). Life cycle sustainability assessment of rc buildings in seismic regions. *Engineering Structures*, *110*, 347–362.

Gomes, L., & Vickery, B. (1977). On the prediction of extreme wind speeds from the parent distribution. *Journal of Wind Engineering and Industrial Aerodynamics*, *2*(1), 21–36.

Hart, G., & Jain, A. (2014). Performance-based wind evaluation and strengthening of existing tall concrete buildings in the los angeles region: dampers, nonlinear time history analysis and structural reliability. *The structural design of tall and special buildings*, *23*, 1256–1274.

Ierimonti, L., Caracoglia, L., Venanzi, I., & Materazzi, A. (2017). Investigation on life-cycle damage cost of wind-excited tall buildings considering directionality effects. *Journal of Wind Engineering and Industrial Aerodynamics*, *171*, 207–218.

Jalayer, F., Asprone, D., Prota, A., & Manfredi, G. (2011). Multi-hazard upgrade decision making for critical infrastructure based on life-cycle cost criteria. *Earthquake Engineering and Structural Dynamics*, *40*(10), 1163–1179.

Jeary, A. (1986). Damping in tall buildings - a mechanism and a predictor. *Earthquake Engineering and Structural Dynamics*, *14*, 733–750.

Kameshwar, S., & Padgett, J. (2014). Multi-hazard risk assessment of highway bridges subjected to earthquake and hurricane hazards. *Engineering Structures*, *78*, 154–166.

Kanduri, A., & Morrow, G. (1996). Damping in structures: its evaluation and treatment of uncertainty. *Journal of Wind Engineering and Industrial Aerodynamics*, *59*, 131–157.

Kaveh, A., Kalateh-Ahani, M., & Fahimi-Farzam, M. (2014). Life-cycle cost optimization of steel moment-frame structures: Performance-based seismic design approach. *Earthquake and Structures*, *7*(3), 271–294.

Lagaros, N. (2007). Life-cycle cost analysis of design practices for rc framed structures. *Bulletin of Earthquake Engineering*, *5*(3), 425–442.

Lagomarsino, S. (1993). Forecast models for damping and vibration periods of buildings. *Journal of Wind Engineering and Industrial Aerodynamics*, *48*, 221–239.

Lavan, O., & Avishur, M. (2013). Seismic behavior of viscously damped yielding frames under structural and damping uncertainties. *Bulletin of Earthquake Engineering*, *11*(6), 2309–2332.

Li, G., & Hu, H. (2014). Risk design optimization using many-objective evolutionary algorithm with application to performance-based wind engineering of tall buildings. *Structural Safety*, *48*, 1–14.

Li, Y., & Van de Lindt, J. W. (2012). Loss-based formulation for multiple hazards with application to residential buildings. *Engineering Structures*, *38*, 123–133.

Liu, M., Wen, Y. K., & Burns, S. (2004). Life cycle cost oriented seismic design optimization of steel moment frame structures with risk-taking preference. *Engineering Structures*, *26*(10), 1407–1421.

Mahmoud, H., & Cheng, G. (2017). Framework for lifecycle cost assessment of steel buildings under seismic and wind hazards. *Journal of Structural Engineering*, *143*(3).

Matta, E. (2015). Seismic effectiveness of tuned mass dampers in a life-cycle cost perspective. *Earthquake and Structure*, *9*(1), 73–91.

McGuire, R. (1995). Probabilistic seismic hazard analysis and design earthquakes: closing the loop. *Bulletin of the Seismological Society of America*, *85*(5), 1275–1284.

Miranda, E., Mosqueda, G., Retamales, R., & Pekcan, G. (2012). Performance of nonstructural components during the 27 February 2010 Chile earthquake. *Earthquake Spectra*, *28*(SUPPL.1), S453–S471.

Mitropoulou, C., Lagaros, N., & Papadrakakis, M. (2015). Generation of artificial accelero-

grams for efficient life-cycle cost analysis of structures. *Engineering Structures*, *88*, 138–153.
Mitropoulou, C. C., Lagaros, N., & Papadrakakis, M. (2011). Life-cycle cost assessment of optimally designed reinforced concrete buildings under seismic actions. *Reliability Engineering and System Safety*, *96*, 1311–1331.
Okasha, N., & Frangopol, D. (2011). Computational platform for the integrated life-cycle management of highway bridges. *Engineering Structures*, *33*(7), 2145–2153.
Padgett, J., Dennemann, K., & Ghosh, J. (2010). Risk-based seismic life-cycle cost-benefit (LCC-B) analysis for bridge retrofit assessment. *Structural Safety*, *32*(3), 165–173.
PEER. (2010). *Tall Buildings Initiative, Guidelines for performance-based seismic design of tall buildings* (Tech. Rep. No. 05). Pacific Earthquake Engineering Research Center.
PEER. (2017). *PEER–NISEE on line library.* `https://nisee.berkeley.edu/elibrary/`.
Priestley, M., Calvi, M., & Kowalsky, M. (2007). *Displacement-based seismic design of structures.* IUSS Press, Pavia, Italy.
Pu, W., Kasai, K., & Kashima, T. (2012). Response of conventional seismic-resistant tall buildings in tokyo during 2011 great east japan earthquake. In *Proceedings of the 15th World Conference on Earthquake Engineering (SFSI 09).* Lisbon, Portugal.
Puthanpurayil, A., Lavan, O., & Dhakal, R. (2015). Seismic loss optimization of nonlinear moment frames retrofitted with viscous dampers. In *Proceedings of the 10th Pacific Conference on Earthquake Engineering (10PCEE).* Sydney, Australia.
Puthanpurayil, A., Lavan, O., & Dhakal, R. (2017). Multi-objective loss optimization of seismic retrofitting of moment resisting frames using viscous dampers. In *Proceedings of the 16th World Conference on Earthquake Engineering (16WCEE).* Santiago, Chile.
Ramirez, C., Liel, A., Mitrani-Reiser, J., Haselton, C., Spear, A., Steiner, J., ... Miranda, E. (2012). Expected earthquake damage and repair costs in reinforced concrete frame buildings. *Earthquake Engineering and Structural Dynamics*, *41*, 1455–1475.
Ramirez, C., & Miranda, E. (2012). Significance of residual drifts in building earthquake loss estimation. *Earthquake Engineering and Structural Dynamics*, *41*(11), 1477–1493.
Rutenberg, A. (1981). A direct p-delta analysis using standard plane frame computer programs. *Computers and Structures*, *14*(1–2), 97–102.
Samali, B., Kwok, K., Wood, G., & Yang, J. (2004). Wind tunnel tests for wind-excited benchmark building. *Journal of Engineering Mechanics*, *130*(4), 447–450.
Satake, N., Suda, K., Arakawa, T., Sasaki, A., & Tamura, Y. (2003). Damping evaluation using full-scale data of buildings in Japan. *Journal of Structural Engineering*, *129*(4), 470–477.
Seo, D., & Caracoglia, L. (2013). Estimating life-cycle monetary losses due to wind hazards: Fragility analysis of long-span bridges. *Engineering Structures*, *56*, 1593–1606.
Spence, S., & Kareem, A. (2014). Performance-based design and optimization of uncertain wind-excited dynamic building systems. *Engineering Structures*, *78*, 133–144.
Stafford Smith, B., & Coull, A. (1991). *Tall building structures: Analysis and design.* John Wiley & Sons.
Taflanidis, A., & Beck, J. (2009). Life-cycle cost optimal design of passive dissipative devices. *Structural Safety*, *31*(6), 508–522.
Venanzi, I. (2015). Robust optimal design of tuned mass dampers for tall buildings with uncertain parameters. *Structural and Multidisciplinary Optimization*, *51*(1), 239–250.
Venanzi, I., & Materazzi, A. (2012). Acrosswind aeroelastic response of square tall buildings: A semi-analytical approach based of wind tunnel tests on rigid models. *Wind and Structures*, *15*(6), 495–508.
Vickery, P., Skerlj, P., Lin, J., Twisdale Jr., L., Young, M., & Lavelle, F. (2006). HAZUS-MH Hurricane Model Methodology. II: Damage and Loss Estimation. *Natural Hazards Review*, *7*(2), 94–103.
Wang, C., Zhai, M., Li, H., Ni, Y., & Guo, T. (2015). Life-cycle cost based maintenance and rehabilitation strategies for cable supported bridges. *Advanced Steel Construction*, *11*(3), 395–410.
Wen, Y. (2001). Minimum lifecycle cost design under multiple hazards. *Reliability Engineering and System Safety*, *73*, 223–231.

Wen, Y., & Kang, Y. (2001a). Minimum building life-cycle cost design criteria. II: Applications. *Journal of Structural Engineering*, *127*(3), 338–346.

Wen, Y., & Kang, Y. (2001b). Minimum building life-cycle cost design criteria. I: Methodology. *Journal of Structural Engineering*, *127*(3), 330–337.

Yang, J., Agrawal, A., Samali, B., & Wu, J. (2004). Bench-mark problem for response control of wind-excited tall building. *Journal of Engineering Mechanics*, *130*(4), 437–446.

Zhou, X., & Xu, Y. (2007). Multi-hazard performance assessment of a transfer-plate high-rise building. *Earthquake Engineering and Engineering Vibration*, *6*(4), 371–382.